# Impacts of Mutual Interference Analysis in FMCW Automotive Radar

Kumbul, Utku; Chen, Yue; Petrov, Nikita ; Vaucher, Cicero S.; Yarovoy, Alexander

**DOI**
10.23919/EuCAP57121.2023.10133503

**Publication date**
2023

**Document Version**
Final published version

**Published in**
Proceedings of the 2023 17th European Conference on Antennas and Propagation (EuCAP)

# Impacts of Mutual Interference Analysis in FMCW Automotive Radar

Utku Kumbul*, Yue Chen*, Nikita Petrov†*, Cicero S. Vaucher†*, Alexander Yarovoy*
* Department of Microelectronics, Delft University of Technology, Delft, The Netherlands
† NXP Semiconductors, Eindhoven, The Netherlands
{u.kumbul, n.petrov, c.silveiravaucher, a.yarovoy}@tudelft.nl

***Abstract*—Mutual interference in the frequency modulated continuous wave (FMCW) radar is studied, and the influence of the FMCW interference on the beat frequency is analyzed. An analytical expression for the victim radar received signal spectrum is derived. Different interference scenarios are investigated by means of interference impact on the range-Doppler profile. It is shown that coherent interference concentrates within multiple range cells while non-coherent interference spreads the interference power over the whole range-Doppler plane.**

***Index Terms*—Automotive radar, Mutual interference, FMCW Radar, Interference Model, Spectrum analysis.**

## I. Introduction

Traffic safety concerns raise a growing interest towards self-driving cars. Automotive radars can function in adverse weather conditions, and thus they play a critical role in advanced driver-assistance systems (ADAS) to realize autonomous driving. Most modern vehicles are already equipped with radar systems to enhance road safety [1]. However, radar-to-radar interference has become an important issue due to the increasing number of automotive radar sensors [2].

Frequency modulated continuous wave (FMCW) can achieve high performance with a low hardware complexity and thus is commonly utilized in automotive radars [1]. The FMCW automotive radar performs the dechirping operation, which leads to a single-tone beat signal per point-like target and keeps the low waveform sampling demands in the radar receiver. Then, target range-Doppler estimation is obtained from the beat signal using a two-dimensional fast Fourier transform (FFT) [3]. However, the FMCW automotive radars suffer from mutual interference [4]–[6]. The structure and characteristics of the mutual interference vary according to the interference signal system parameters [7]. Thus, the relationship between the mutual interference signal parameters and their effect on the radar system performance needs to be understood for developing proper interference estimation or machine learning methods. To this end, many studies have been conducted to analyze and model the mutual interference problem between FMCW automotive radars [8]–[13]. Particularly, a generalized radar-to-radar interference equation is proposed to analytically describe as many scenarios as possible in [13]. Therein, the victim radar beat signal is derived in the time domain for different waveform types. The main motivation of this study is to revisit the present detailed analysis of the FMCW radar in the time domain and extend it into the frequency spectrum.

In this paper, we analytically investigate the FMCW automotive radar mutual interference problem and derive the victim radar spectrum in the beat frequency. Subsequently, we examine the effects of different interference scenarios on the victim radar system performance. In order to achieve this task, we give the signal model of interfered FMCW radar before processing in Section II. Then, we analyze the spectrum of the victim radar in Section III. Then, we investigate different interference cases and demonstrate their influence on the range-Doppler profile in Section IV. Finally, the conclusions are presented in Section V.

## II. Signal Model

The transmitted FMCW signal of the victim radar can be given as:

$$s_{\mathrm{t}}(t) = \sqrt{P_{\mathrm{t}}}\exp\left(-j2\pi\left(f_c t + \frac{kt^2}{2}\right)\right), \tag{1}$$

where $P_{\mathrm{t}}$ is the transmit signal power, $k = B/T$ is the chirp rate, $B$ is the chirp bandwidth, $T$ is the chirp duration, and $f_c$ is the carrier frequency of the victim radar. The received FMCW signal reflected from a target can be represented as:

$$s_{\mathrm{r_{tar}}}(t) = \alpha_{\mathrm{tar}}\exp\left(-j2\pi\left(f_c(t-\tau) + \frac{k(t-\tau)^2}{2}\right)\right), \tag{2}$$

where $\tau$ is the time delay between the victim radar and the target, $\alpha_{\mathrm{tar}} = e^{j\varphi_0}\sqrt{P_{\mathrm{tar}}}$ is the amplitude of the received target echo, $P_{\mathrm{tar}}$ is the received power of the target echo, and $e^{j\varphi_0}$ is a constant phase term due to two-way propagation of the wave and the scattering coefficient from the target. For the FMCW interfering sensor, the received interference signal can be written as:

$$s_{\mathrm{r_i}}(t) = \alpha_{\mathrm{i}}\exp\left(-j2\pi\left(f_{c_{\mathrm{i}}}(t-\tau_{\mathrm{i}}) + \frac{k_{\mathrm{i}}(t-\tau_{\mathrm{i}})^2}{2}\right)\right), \tag{3}$$

where $\tau_{\mathrm{i}}$ is the time delay between the victim and interfering sensors, $\alpha_{\mathrm{i}} = e^{j\varphi_{\mathrm{i}}}\sqrt{P_{\mathrm{i}}}$ is the amplitude of received interference, $P_{\mathrm{i}}$ is the received power of the interference signal, $e^{j\varphi_{\mathrm{i}}}$ is a constant phase term due to one-way propagation and the initial phase of the interference, $k_{\mathrm{i}}$ is the chirp slope, and $f_{c_{\mathrm{i}}}$ is the carrier frequency of the interfering radar. We assume the interference signal is present during the victim radar chirp duration for derivations. The received signal powers can be defined as:

$$P_{\mathrm{tar}} = \frac{P_t G_t G_r \lambda^2 \sigma}{(4\pi)^3 R^4_{\mathrm{tar}}}, \tag{4}$$

and

$$P_{\mathrm{i}} = \frac{P_{\mathrm{t_i}} G_{t_{\mathrm{i}}} G_r {\lambda_{\mathrm{i}}}^2}{(4\pi)^2 {R_{\mathrm{i}}}^2}, \tag{5}$$

where $R_{\mathrm{tar}}$ is the target range, $\sigma$ is the target's radar cross-section, $\lambda$ is the wavelength, $G_t$ and $G_r$ are the transmitting and receiving antenna gains of the victim radar. Similarly, $R_{\mathrm{i}}$ is the range between the interfering and victim radar, $P_{t_{\mathrm{i}}}$ is the transmit power, $\lambda_{\mathrm{i}}$ is the wavelength, and $G_{t_{\mathrm{i}}}$ is the transmitting antenna gain of the interference radar, respectively. The total received signal in the victim radar is dechirped by multiplying it with the complex conjugate of the reference transmit signal associated with the victim radar. Then, the resulting beat signal becomes:

$$\begin{aligned} s_{\mathrm{b}}(t) &= \left(s_{\mathrm{r_{tar}}}(t) + s_{\mathrm{r_i}}(t)\right) e^{j2\pi\left(f_c t + \frac{kt^2}{2}\right)} \\ &= \alpha_{\mathrm{tar}}\, e^{j2\pi\left(f_c\tau + k\tau t - \frac{k\tau^2}{2}\right)} \\ &+ \alpha_{\mathrm{i}}\, e^{j2\pi\left(f_{c_{\mathrm{i}}}\tau_{\mathrm{i}} + (f_c - f_{c_{\mathrm{i}}} + k_{\mathrm{i}}\tau_{\mathrm{i}})t + (\frac{k-k_{\mathrm{i}}}{2})t^2 - \frac{k_{\mathrm{i}}{\tau_{\mathrm{i}}}^2}{2}\right)} \\ &= s_{\mathrm{b_{tar}}}(t) + s_{\mathrm{b_i}}(t). \end{aligned} \tag{6}$$

The dechirped signal has two main components: a single-tone beat signal regarding the target response and an additional signal with a quadratic time component due to interference.

## III. Spectral Analysis

In this section, we analyze the spectrum of the dechirped signal and examine the influence of interference on the victim radar's range and range-Doppler profile.

### A. Effects on the Range Profile

We take the Fourier transform of the dechirped signal (6) to investigate the effect of interference on the range profile. After dechirping, the target beat signal starts at $\tau$ and ends at $T$. For the interference beat signal, we denote $t_1$ and $t_2$ as the starting and ending time instances of the dechirping process between captured interference signal and the reference transmit signal. The dechirped signal in the frequency domain can be written as:

$$S_{\mathrm{b}}(f_1) = S_{\mathrm{b_{tar}}}(f_1) + S_{\mathrm{b_i}}(f_1). \tag{7}$$

By taking the Fourier transform, the spectrum of the target beat signal can be represented as:

$$\begin{aligned} S_{\mathrm{b_{tar}}}(f_1) &= \alpha_{\mathrm{tar}} \int_{\tau}^{T} e^{j2\pi\left(f_c\tau + k\tau t - \frac{1}{2}k\tau^2\right)} e^{-j2\pi f_1 t} dt \\ &= \alpha_{\mathrm{tar}}\, e^{j2\pi\left(f_c\tau - \frac{1}{2}k\tau^2\right)} \frac{\left(e^{j2\pi(k\tau - f_1)T} - e^{j2\pi(k\tau - f_1)\tau}\right)}{j2\pi(k\tau - f_1)}. \end{aligned} \tag{8}$$

By substituting $\gamma = k_{\mathrm{i}} - k$ and $\beta = (f_c - f_{c_{\mathrm{i}}} - f_1 + k_{\mathrm{i}}\tau_{\mathrm{i}})$, the spectrum of the interference beat signal can be obtained as:

$$\begin{aligned} &S_{\mathrm{b_i}}(f_1) = \alpha_{\mathrm{i}} \\ &\int_{t_1}^{t_2} e^{j2\pi\left(f_{c_{\mathrm{i}}}\tau_{\mathrm{i}} + (f_c - f_{c_{\mathrm{i}}} + k_{\mathrm{i}}\tau_{\mathrm{i}})t + (\frac{k-k_{\mathrm{i}}}{2})t^2 - \frac{k_{\mathrm{i}}{\tau_{\mathrm{i}}}^2}{2}\right)} e^{-j2\pi f_1 t} dt \\ &= \alpha_{\mathrm{i}} e^{j2\pi\left(f_{c_{\mathrm{i}}}\tau_{\mathrm{i}} - \frac{k_{\mathrm{i}}{\tau_{\mathrm{i}}}^2}{2}\right)} e^{\left(\frac{j\pi\beta}{\sqrt{j\pi\gamma}}\right)^2} \int_{t_1}^{t_2} e^{-\left(\sqrt{j\pi\gamma}t - \frac{j\pi\beta}{\sqrt{j\pi\gamma}}\right)^2} dt \\ &= \alpha_{\mathrm{i}} \frac{e^{j2\pi\left(f_{c_{\mathrm{i}}}\tau_{\mathrm{i}} - \frac{k_{\mathrm{i}}{\tau_{\mathrm{i}}}^2}{2}\right)}}{2\sqrt{j(k_{\mathrm{i}} - k)}} e^{\left(\frac{j\pi(f_c - f_{c_{\mathrm{i}}} - f_1 + k_{\mathrm{i}}\tau_{\mathrm{i}})}{\sqrt{j\pi(k_{\mathrm{i}} - k)}}\right)^2} \\ &\left(\mathrm{erf}\left(\sqrt{j\pi(k_{\mathrm{i}} - k)}t_2 - \frac{j\pi(f_c - f_{c_{\mathrm{i}}} - f_1 + k_{\mathrm{i}}\tau_{\mathrm{i}})}{\sqrt{j\pi(k_{\mathrm{i}} - k)}}\right)\right. \\ &\left. -\mathrm{erf}\left(\sqrt{j\pi(k_{\mathrm{i}} - k)}t_1 - \frac{j\pi(f_c - f_{c_{\mathrm{i}}} - f_1 + k_{\mathrm{i}}\tau_{\mathrm{i}})}{\sqrt{j\pi(k_{\mathrm{i}} - k)}}\right)\right), \end{aligned} \tag{9}$$

where erf is the error function. The beat frequency component in the resulting signal can be converted to range as:

$$R = \frac{cT}{2B} f_1, \tag{10}$$

where the positive frequency bins span $0 \le f_1 \le f_s/2$ and the associated range bins span $0 \le R \le R_{\mathrm{max}}$ for a given sampling frequency $f_s$. The relationship between the interference spectral characteristic and the resulting interference effect can be seen in (9). In the case of $k_{\mathrm{i}} \neq k$, the error functions cause a chirp-like signal with the combination of two ripples while the error functions start to create a sinc-like response, as $k_{\mathrm{i}}$ approaches to $k$.

### B. Effects on the Range-Doppler Profile

In the FMCW automotive radars, multiple chirp pulses are used for velocity estimation. In the case of having different chirp duration, the starting time instance of captured interference will be different for each chirp pulse, resulting in non-coherent interference. Thus, it is difficult to model such a scenario. However, the coherent interference case, where the victim and interfering sensors have the same chirp duration, can be modelled to derive an analytical expression for the range-Doppler profile. Assume both victim and interfering radars transmit $N_p$ number of pulses with a chirp duration $T$. The velocity difference among the chirp pulses introduces a term $\exp(j2\pi f_d m T)$, where $f_d$ is the Doppler frequency shift and $m$ is the index of chirp pulses (slow-time) as $0 \le m \le N_p - 1$. Then, the fast-time and slow-time representation of dechirped signal (6) can be recast as:

$$\begin{aligned} s_{\mathrm{b}}(t, m) &= \alpha_{\mathrm{tar}}\, e^{j2\pi\left(f_c\tau + k\tau t - \frac{k\tau^2}{2}\right)} e^{j2\pi f_{\mathrm{d_t}} m T} \\ &+ \alpha_{\mathrm{i}} e^{j2\pi\left(f_{c_{\mathrm{i}}}\tau_{\mathrm{i}} + (f_c - f_{c_{\mathrm{i}}} + k_{\mathrm{i}}\tau_{\mathrm{i}})t + (\frac{k-k_{\mathrm{i}}}{2})t^2 - \frac{k_{\mathrm{i}}{\tau_{\mathrm{i}}}^2}{2}\right)} e^{j2\pi f_{\mathrm{d_i}} m T}. \end{aligned} \tag{11}$$

To obtain the range-Doppler profile, we take the first Fourier transform along the fast-time and then the second Fourier

transform along the slow-time. The resulting two-dimensional Fourier transform of the target and interference beat signals can be written as:

$$S_{\mathrm{b_{tar}}}(f_1, f_2) = \alpha_{\mathrm{tar}}\, e^{j2\pi\left(f_c\tau - \frac{1}{2}k\tau^2\right)} \frac{\left(e^{j2\pi(k\tau - f_1)T} - e^{j2\pi(k\tau - f_1)\tau}\right)}{j2\pi(k\tau - f_1)} \frac{\left(e^{\left(j2\pi\left(f_{\mathrm{d_t}}T - f_2\right)(N_p - 1)\right)} - 1\right)}{j2\pi\left(f_{\mathrm{d_t}}T - f_2\right)}, \tag{12}$$

and

$$S_{\mathrm{b_i}}(f_1, f_2) = \alpha_{\mathrm{i}} \frac{e^{j2\pi\left(f_{c_{\mathrm{i}}}\tau_{\mathrm{i}} - \frac{k_{\mathrm{i}}\tau_{\mathrm{i}}^2}{2}\right)}}{2\sqrt{j(k_{\mathrm{i}} - k)}} e^{\left(\frac{j\pi(f_c - f_{c_{\mathrm{i}}} - f_1 + k_{\mathrm{i}}\tau_{\mathrm{i}})}{\sqrt{j\pi(k_{\mathrm{i}} - k)}}\right)^2} \left(\mathrm{erf}\left(\sqrt{j\pi(k_{\mathrm{i}} - k)}t_2 - \frac{j\pi(f_c - f_{c_{\mathrm{i}}} - f_1 + k_{\mathrm{i}}\tau_{\mathrm{i}})}{\sqrt{j\pi(k_{\mathrm{i}} - k)}}\right) - \mathrm{erf}\left(\sqrt{j\pi(k_{\mathrm{i}} - k)}t_1 - \frac{j\pi(f_c - f_{c_{\mathrm{i}}} - f_1 + k_{\mathrm{i}}\tau_{\mathrm{i}})}{\sqrt{j\pi(k_{\mathrm{i}} - k)}}\right)\right) \frac{\left(e^{\left(j2\pi\left(f_{\mathrm{d_i}}T - f_2\right)(N_p - 1)\right)} - 1\right)}{j2\pi\left(f_{\mathrm{d_i}}T - f_2\right)}, \tag{13}$$

where $f_{\mathrm{d_t}} = \frac{2v_{\mathrm{tar}}}{\lambda}$ and $v_{\mathrm{tar}}$ is the target velocity. Note that the interference signal has one-way propagation, and hence its Doppler frequency shift $f_{\mathrm{d_i}} = \frac{v_{\mathrm{i}}}{\lambda_{\mathrm{i}}}$, where $v_{\mathrm{i}}$ is the relative velocity between victim and interfering sensors.

## IV. Simulations

The captured interference can be coherent, periodically coherent, and non-coherent based on the interferer radar system parameters. In this section, we investigate different FMCW automotive radar interference scenarios and simulate their impacts on the victim radar's range-Doppler profile. Assume a victim radar operates at carrier frequency $f_c = 77$ GHz and transmits $N_p = 256$ chirp pulses with a chirp duration $T = 25.6$ $\mu$s and chirp bandwidth $B = 200$ MHz. Consider the transmitted signal is reflected from a target at $R = 50$ m with a radial velocity $v = 20$ m/s and received along with the complex Gaussian noise. We set the signal-to-noise ratio (SNR) as SNR $= -10$ dB. In addition, assume the FMCW interferer radar operating at carrier frequency $f_{c_{\mathrm{i}}} = 77$ GHz is located at $R_{\mathrm{i}} = 250$ m with a radial velocity $v_{\mathrm{i}} = 40$ m/s, and an additional interference signal is captured for every chirp pulses. We set the received interference signal amplitude $\alpha_{\mathrm{i}} = 4\alpha_{\mathrm{tar}}$, i.e. the received interference signal power is 12 dB higher than the received target signal power. Then, the total received signal is downconverted to the baseband. The received signal in the baseband is dechirped and filtered by Hamming low-pass filter (LPF) with the cut-off frequency $f_{cut} = \pm 40$ MHz. Then, ADC with the sampling frequency $f_s = 80$ MHz is used to sample the beat signal. Moreover, we apply 80 dB Chebyshev window to the sampled signal and then process the windowed signal using the two-dimensional FFT.

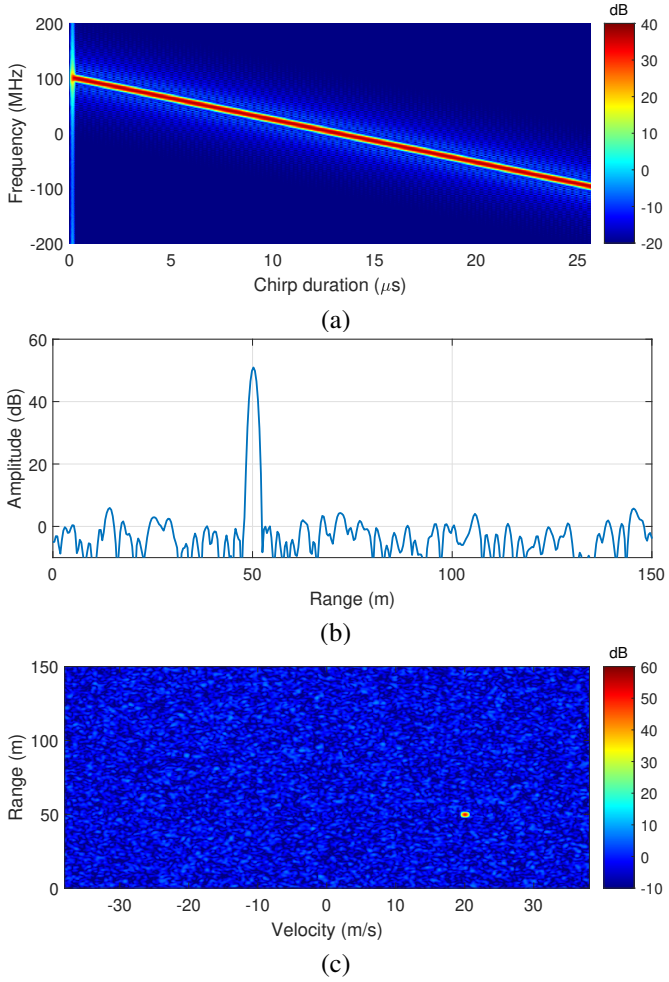


Fig. 1. FMCW Radar: No interference scenario. (a) Spectrogram of the received signal in baseband. (b) Range profile. (c) Range-Doppler profile.

First, we examine the sensing performance of the victim radar in an interference-free scenario, as shown in Fig. 1. For comparison of the instantaneous frequency in different scenarios, we illustrate the spectrogram of the received signal (first pulse) in the baseband (Fig. 1 a). To highlight the instantaneous frequency behaviour, all spectrogram figures of the received signal are shown for a noise-free case. Then, we process the received signal with noise and demonstrate the range and range-Doppler profile of the victim radar in Fig. 1 b and c. Note that there is a signal processing gain (increase in SNR) as $10\log_{10}(BT) + 10\log_{10}(N_p) = 61$ dB after range-Doppler processing. The noise level is estimated from the target-free Doppler cell and used to normalize the range response of the target. It is seen that the dynamic range is around $\sim 51$ dB for the target in an interference-free case.

Then, we investigate the impacts of the coherent FMCW interference in Fig. 2. In this interference scenario, the chirp duration of the interference needs to be the same as the victim radar chirp duration, while the interference radar has a different chirp slope. To realize such a scenario, we set the interference chirp duration $T_{\mathrm{i}} = 25.6$ $\mu$s and chirp bandwidth

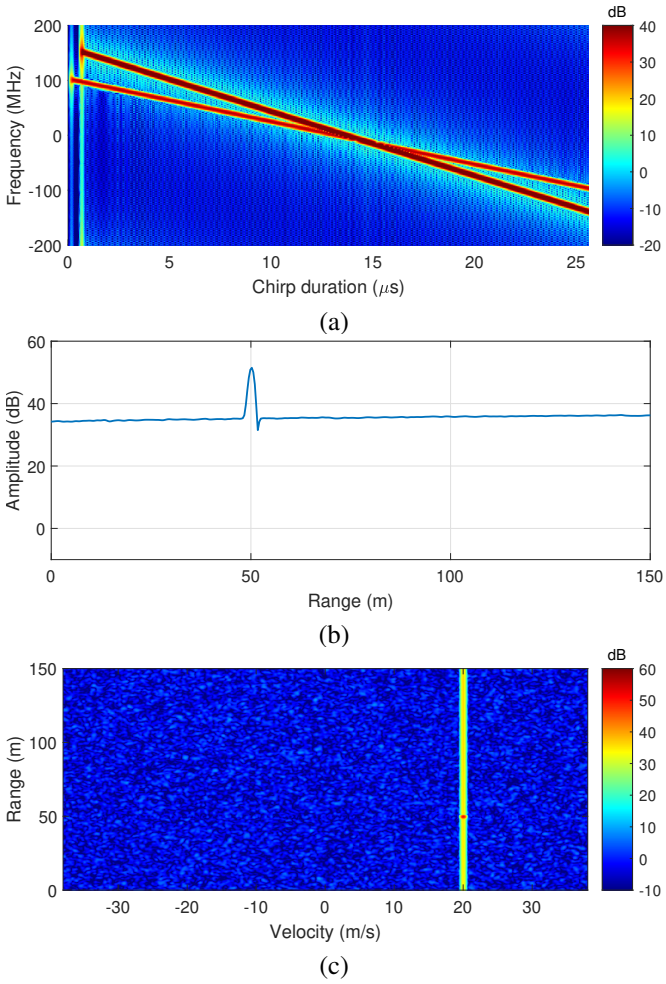


Fig. 2. FMCW Radar: Coherent interference scenario. (a) Spectrogram of the received signal in baseband. (b) Range profile. (c) Range-Doppler profile.

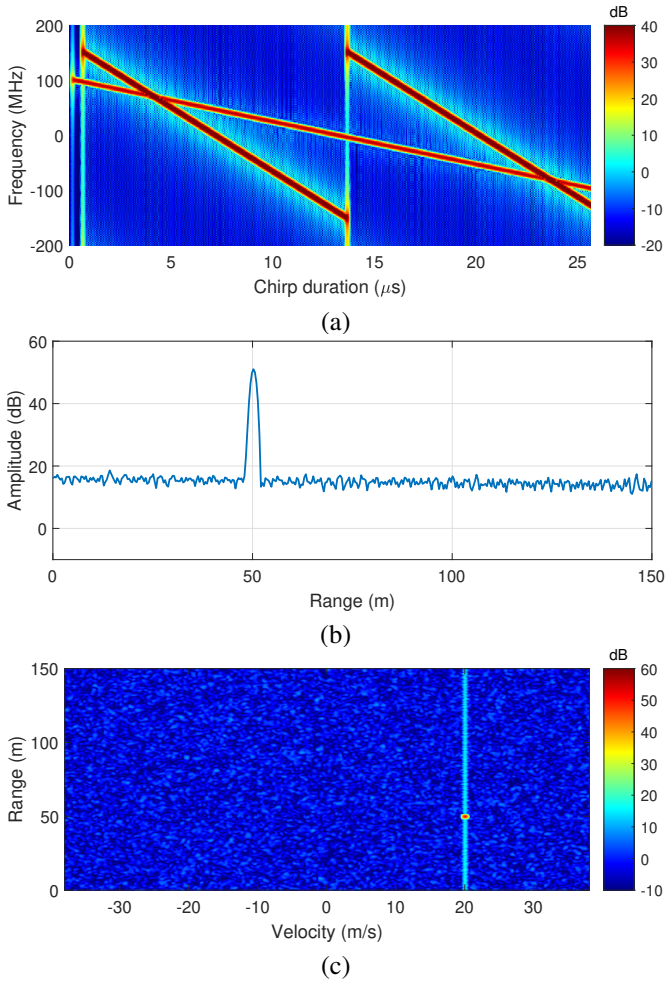


Fig. 3. FMCW Radar: Periodically coherent interference scenario. (a) Spectrogram of the received signal in baseband. (b) Range profile. (c) Range-Doppler profile.

$B_{\mathrm{i}} = 300$ MHz. It can be seen that the received interference signal in the baseband spans the frequency between $\pm 150$ MHz and overlaps with the received chirp signal of the victim radar (Fig. 2 a). Therefore, dechirping the interference with the reference transmit signal leads to a so-called "V-shape" or a diagonal line in the dechirped signal spectrogram [13]. Since the interference has the same chirp duration, the location of such a diagonal line or "V-shape" is the same for every chirp pulses. As a result, this interference type affects only the range profile, and the interference power is spread over the multiple range bins. This behaviour can be seen in Fig. 2 b, where the interference power is spread over the range profile. We observe that the dynamic range degraded to $\sim 16$ dB, and the range profile of the victim radar heavily suffers from such an interference case. Notice that the chirp slopes are different, and hence the wide-band interference occurs in this coherent case. On the other hand, the interference becomes narrow-band interference as the interference chirp slope approaches $k$, and the ghost target scenario occurs in the fully coherent case. However, such a ghost target scenario is unlikely to be generated by other radars in the environment.

Next, we demonstrate the effects of the periodically coherent FMCW interference in Fig. 3, where the interference chirp duration is multiples of the victim radar chirp duration. To this end, we set the interference chirp duration $T_{\mathrm{i}} = 12.8$ $\mu$s with a chirp bandwidth $B_{\mathrm{i}} = 300$ MHz. In this case, the interference appears at the same location for every chirp pulse, but its duration becomes half, intersecting with the victim radar two times in the instantaneous frequency (Fig. 3 a). Thus, the interference power spread over a range profile similar to the previous case. However, the power of interference is almost halved as some part of the interference beat signal is filtered by LPF, and the remaining energy is on the negative side of the range-Doppler spectrum. As shown in Fig. 3 b, the interference power increase the noise floor around $\sim 18$ dB, and the dynamic range becomes 33 dB.

Finally, we investigate the impacts of the non-coherent FMCW interference scenario in Fig. 4. This interference case occurs when the chirp duration of the interference is aperiodically different than the victim radar chirp duration. Such interference is the most common scenario between automotive

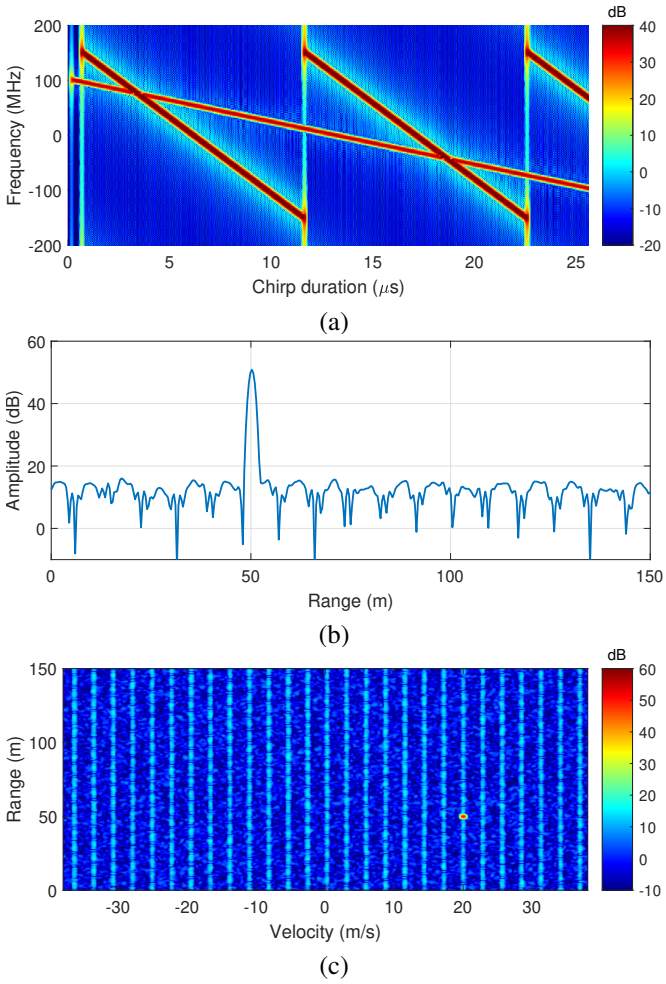


Fig. 4. FMCW Radar: Non-coherent interference scenario. (a) Spectrogram of the received signal in baseband. (b) Range profile. (c) Range-Doppler profile.

radars since the starting point of the mutual interference can be an arbitrary time instance. To mimic this scenario, we set the interference chirp duration $T_{\mathrm{i}} = 10.8$ $\mu$s with a chirp bandwidth $B_{\mathrm{i}} = 300$ MHz. In Fig. 4 a, we demonstrate the spectrogram of the received signal in the baseband for the first pulse. It is important to note that the locations of the overlap position change for every chirp pulse, and the interference chirp signal can overlap multiple times in this scenario. Consequently, the resulting dechirped interference signal is different in each chirp pulse, which leads to spread interference power over both range and Doppler bins. As seen in Fig. 4 c, the non-coherent interference scenario increases the noise floor in multiple Doppler and range cells. In particular, the noise floor in the vicinity of the target is around $\sim 13$ dB, and thus the dynamic range becomes 38 dB.

## V. Conclusion

The mutual interference problem in FMCW automotive radars has been studied analytically. Only one interference signal is considered to investigate the impact of synchronization between the interferer and victim radar. We derive the spectrum of the target response and interference signals in the beat frequency. The derived equation can be utilized to model and approximate the interference spectrum rapidly. Afterwards, the impacts of the mutual interference on the victim radar's range and range-Doppler profile are examined. Degradation in the sensing performance due to the coherent, periodically coherent and non-coherent FMCW interference scenarios are demonstrated via numerical simulations. It is shown that the coherent and periodically coherent interference cases increase the noise floor along the same Doppler bins, while in the case of non-coherent interference, the interference power is spread over multiple range-Doppler cells.

## Acknowledgment

Part of this research activity was performed within the TU Delft Industry Partnership Program (TIPP), which is funded by NXP Semiconductors N.V. and Holland High Tech Systems and Materials (TKIHTSM/18.0136) under the project 'Coded Radar for Interference Suppression in Super-Dense Environments' (CRUISE).

## References

[1] I. Bilik, O. Longman, S. Villeval, and J. Tabrikian, "The rise of radar for autonomous vehicles: Signal processing solutions and future research directions," *IEEE Signal Processing Magazine*, vol. 36, no. 5, pp. 20–31, 2019.

[2] M. Kunert, H. Meinel, C. Fischer, and M. Ahrholdt, "Report on interference density increase by market penetration forecast," in *MOSARIM Consortium, CNTR, Tech. Rep. D1.6, Sep.*, 2010.

[3] F. Roos, J. Bechter, C. Knill, B. Schweizer, and C. Waldschmidt, "Radar sensors for autonomous driving: Modulation schemes and interference mitigation," *IEEE Microwave Magazine*, vol. 20, no. 9, pp. 58–72, 2019.

[4] G. M. Brooker, "Mutual interference of millimeter-wave radar systems," *IEEE Transactions on Electromagnetic Compatibility*, vol. 49, no. 1, pp. 170–181, 2007.

[5] M. Goppelt, H. . Blöcher, and W. Menzel, "Analytical investigation of mutual interference between automotive fmcw radar sensors," in *2011 German Microwave Conference*, 2011, pp. 1–4.

[6] A. Bourdoux, K. Parashar, and M. Bauduin, "Phenomenology of mutual interference of fmcw and pmcw automotive radars," in *2017 IEEE Radar Conference (RadarConf)*, 2017, pp. 1709–1714.

[7] S. Alland, W. Stark, M. Ali, and M. Hegde, "Interference in automotive radar systems: Characteristics, mitigation techniques, and current and future research," *IEEE Signal Processing Magazine*, vol. 36, no. 5, pp. 45–59, 2019.

[8] T. Schipper, S. Prophet, M. Harter, L. Zwirello, and T. Zwick, "Simulative prediction of the interference potential between radars in common road scenarios," *IEEE Transactions on Electromagnetic Compatibility*, vol. 57, no. 3, pp. 322–328, 2015.

[9] A. Al-Hourani, R. J. Evans, S. Kandeepan, B. Moran, and H. Eltom, "Stochastic geometry methods for modeling automotive radar interference," *IEEE Transactions on Intelligent Transportation Systems*, vol. 19, no. 2, pp. 333–344, 2018.

[10] M. Toth, P. Meissner, A. Melzer, and K. Witrisal, "Analytical investigation of non-coherent mutual fmcw radar interference," in *2018 15th European Radar Conference (EuRAD)*, 2018, pp. 71–74.

[11] F. Norouzian, A. Pirkani, E. Hoare, M. Cherniakov, and M. Gashinova, "Phenomenology of automotive radar interference," *IET Radar, Sonar & Navigation*, vol. 15, no. 9, pp. 1045–1060, 2021. [Online]. Available: https://ietresearch.onlinelibrary.wiley.com/doi/abs/10.1049/rsn2.12096

[12] L. L. Tovar Torres, M. Steiner, and C. Waldschmidt, "Channel influence for the analysis of interferences between automotive radars," in *2020 17th European Radar Conference (EuRAD)*, 2021, pp. 266–269.

[13] U. Kumbul, F. Uysal, C. S. Vaucher, and A. Yarovoy, "Automotive radar interference study for different radar waveform types," *IET Radar, Sonar & Navigation*, vol. 16, no. 3, pp. 564–577, 2022. [Online]. Available: https://ietresearch.onlinelibrary.wiley.com/doi/abs/10.1049/rsn2.12203